



*Workshop on “Heusler Alloys for Spintronic Devices”
July 30, 2015 @C-SPIN, Univ. of Minnesota, Minneapolis, USA*

CPP-GMR and Related Phenomena in Half-Metallic Heusler Alloy Systems

Koki Takanashi

**Magnetic Materials Laboratory
Institute for Materials Research (IMR)
Tohoku University
Sendai, Japan**



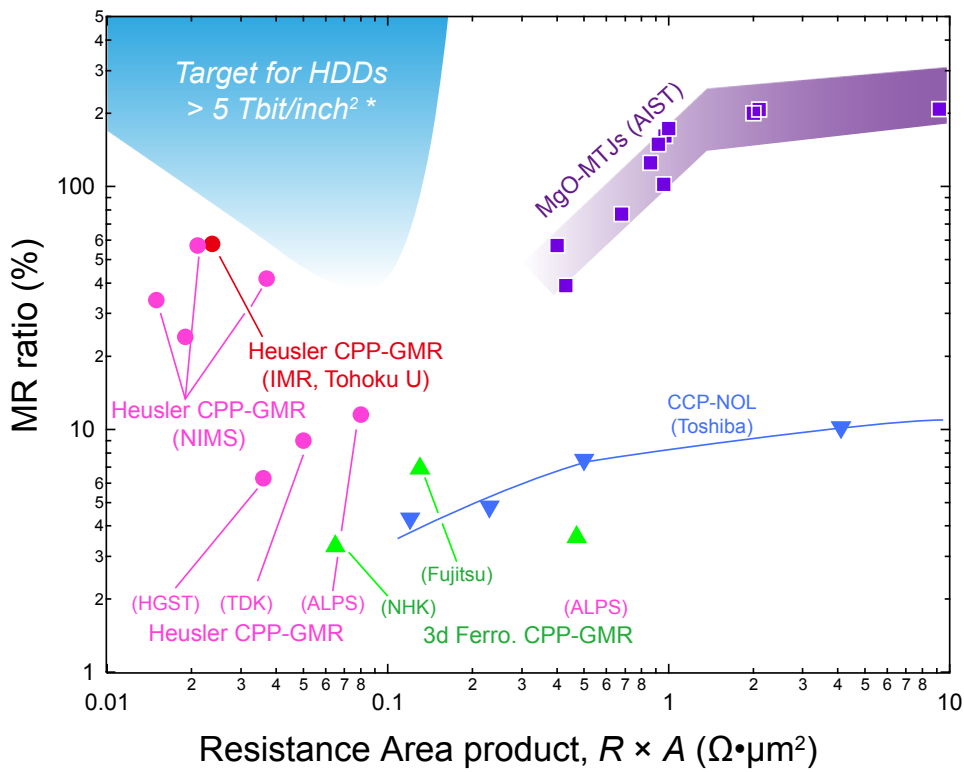
1

Research activities on Heusler alloys in my group

- ***CPP-GMR*** with $\text{Co}_2\text{Fe}_{1-x}\text{Mn}_x\text{Si}$ electrodes
- ***Spin torque oscillation*** with CPP-GMR devices
- ***Giant Peltier effect*** in CPP-GMR devices
- ***Perpendicular magnetization*** of
Heusler alloy thin films
- ***Antiferromagnetic*** Heusler alloy films
to replace IrMn in spin valves

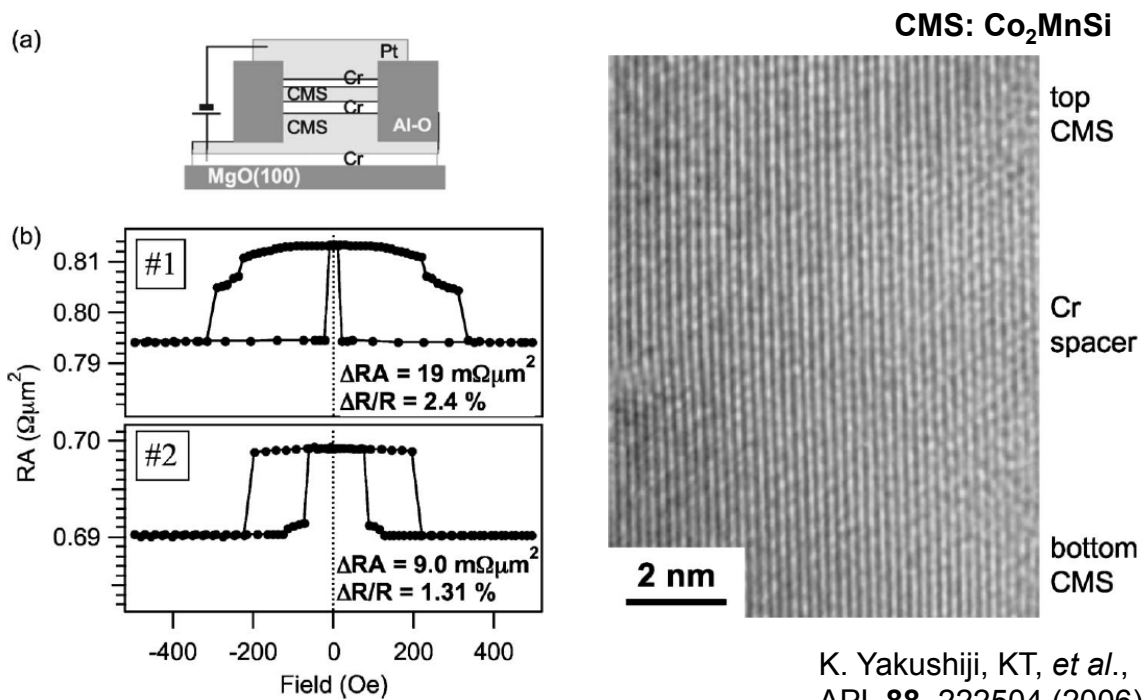
2

High MR ratio with low resistance



3

CMS/Cr/CMS fully-epitaxial CPP-GMR device

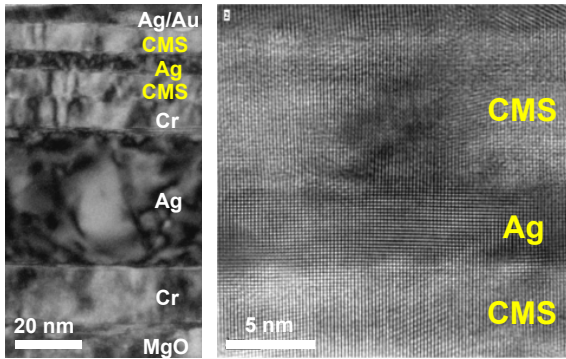
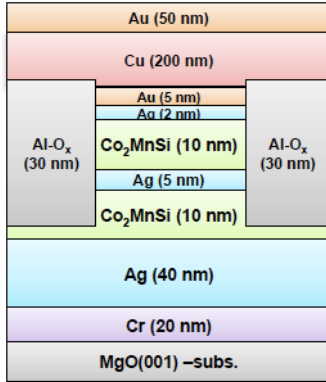


K. Yakushiji, KT, *et al.*,
APL **88**, 222504 (2006).

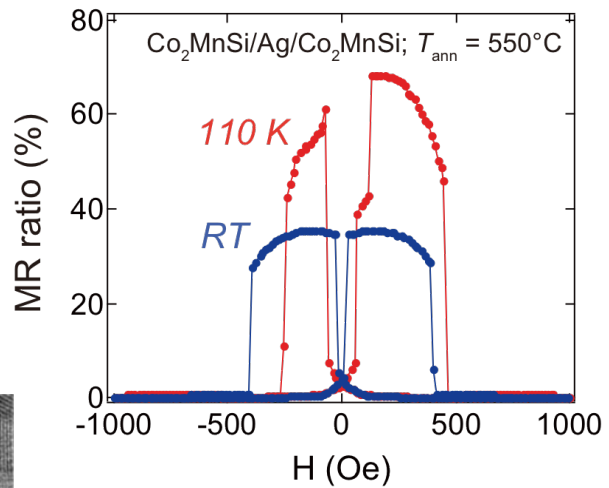
The first experimental report on Heusler-based CPP-GMR devices with large ΔRA values.

4

CMS/Ag/CMS fully-epitaxial CPP-GMR device



Fully-epitaxial growth in CMS/Ag/CMS



Breakthrough of CPP-GMR

A high MR ratio (**36.4%@RT**) was observed.

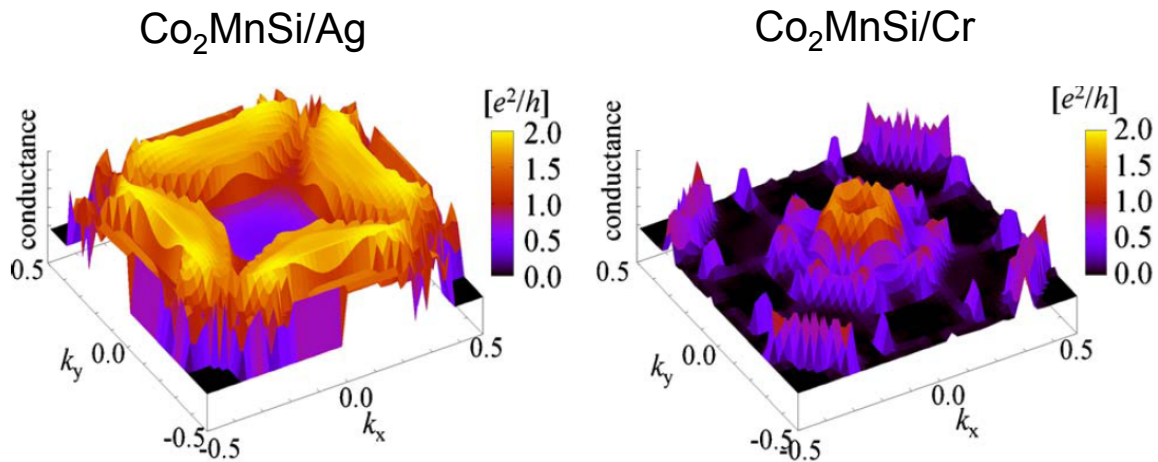
T. Iwase, KT *et al.*, Appl. Phys. Exp., 2 (2009) 063003.
Y. Sakuraba, KT *et al.*, Phys. Rev. B82 (2010) 094444.

5

Ag spacer? or Cr spacer?

Majority spin conductance in the parallel state

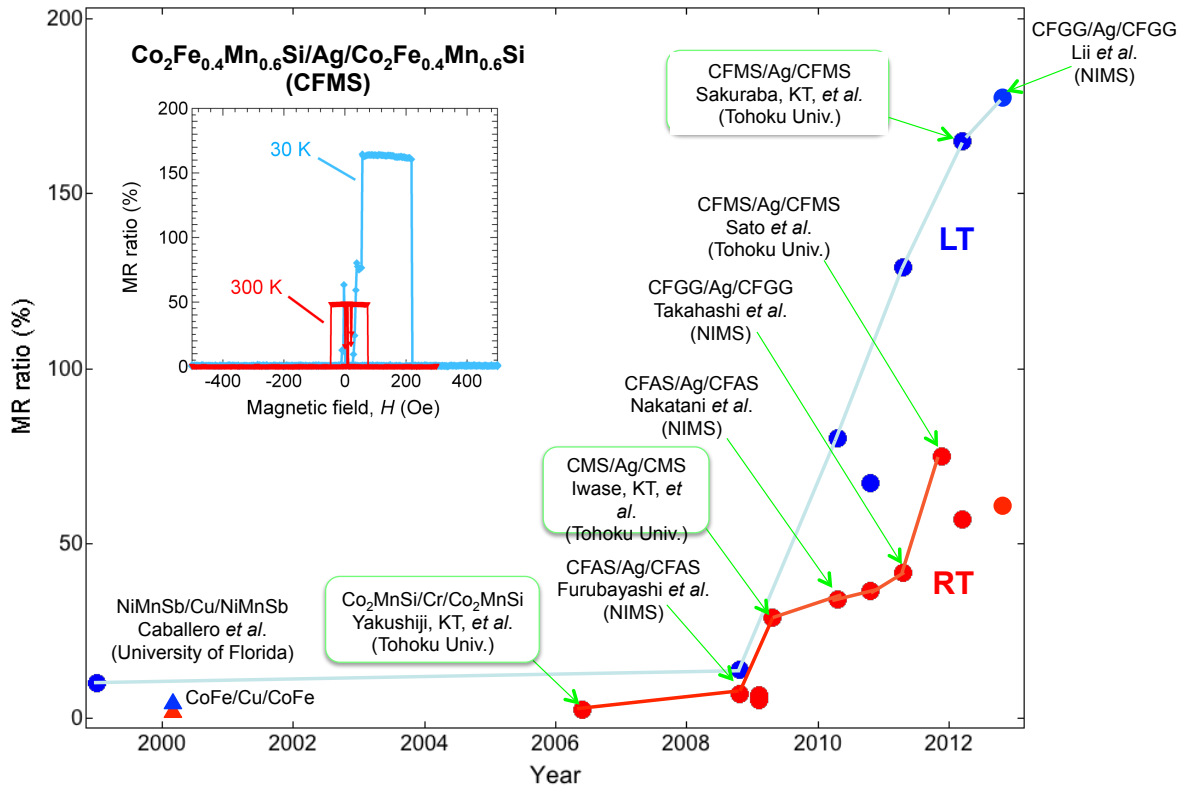
Sakuraba, Miura, KT, *et al.*,
PRB **82**, 094444 (2010).



Matching of the Fermi surface is important.

6

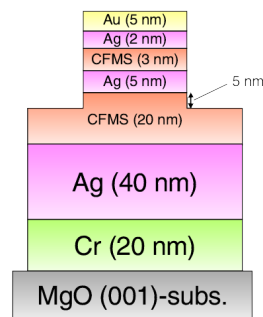
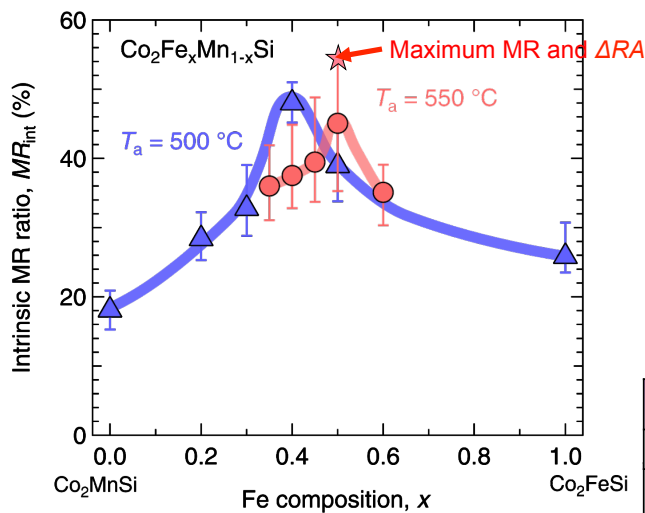
Development of CPP-GMR for Heusler alloys



7

CPP-GMR with Co₂Fe_xMn_{1-x}Si electrodes

Fe:Mn composition ratio x dependence



T_a	x_{best}	MR_{int}	RA	ΔRA
500	0.4	51 %	25.1 $\text{m}\Omega \cdot \mu\text{m}^2$	12.8 $\text{m}\Omega \cdot \mu\text{m}^2$
550	0.5	55 %	31.4 $\text{m}\Omega \cdot \mu\text{m}^2$	17.2 $\text{m}\Omega \cdot \mu\text{m}^2$

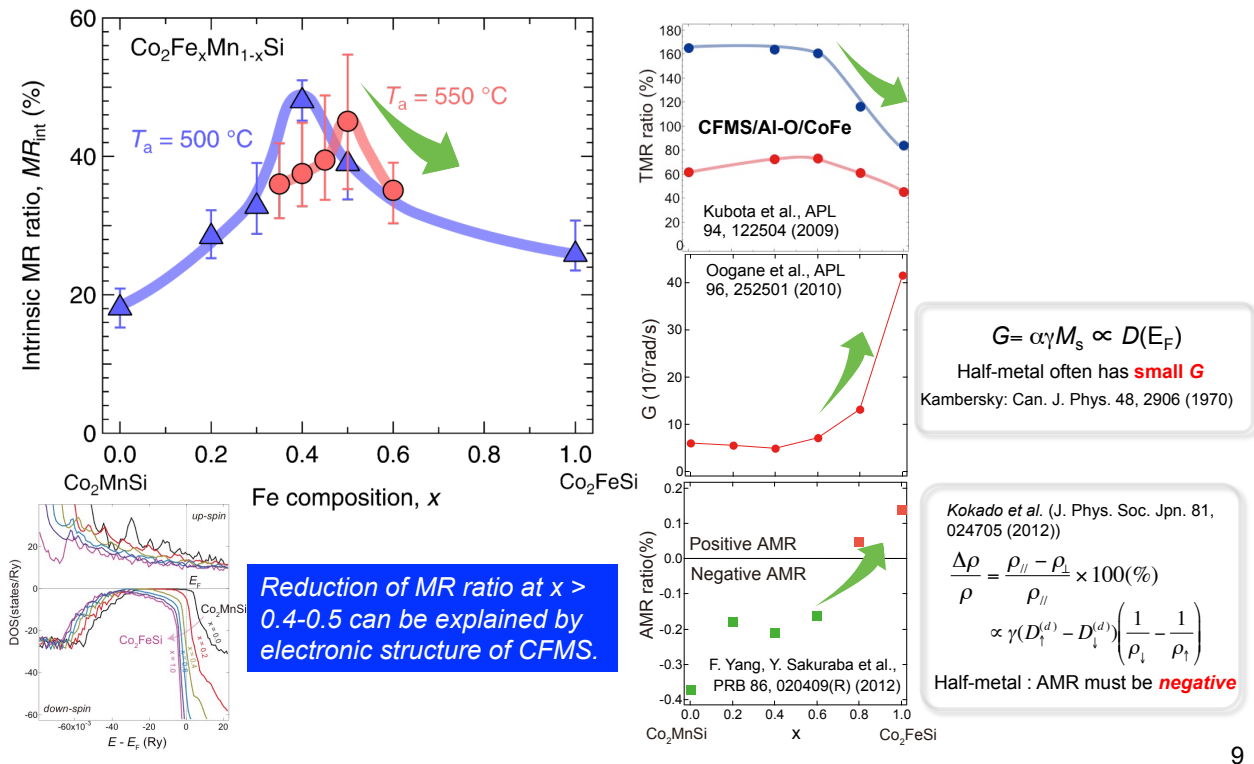
Y. Sakuraba, M. Ueda et al. Appl. Phys. Lett. **101**, 252408(2012).

- The best composition $x = 0.4$ at $T_a = 500^\circ\text{C}$
 0.5 at $T_a = 550^\circ\text{C}$
- The highest ΔRA of $17.2 \text{ m}\Omega \cdot \mu\text{m}^2$ was observed in $\text{Co}_2\text{Fe}_{0.5}\text{Mn}_{0.5}\text{Si}$.

8

CPP-GMR with $\text{Co}_2\text{Fe}_x\text{Mn}_{1-x}\text{Si}$ electrodes

Discussion - Fe:Mn composition ratio x dependence ($x > 0.4-0.5$)

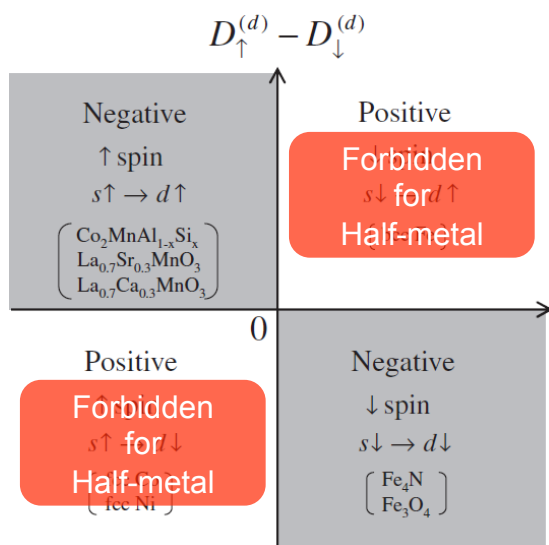


9

Half-metallic materials & AMR effect

s-d scattering procedures and the sign of AMR ratio

S. Kokado, et al., JPSJ 81, 024705 (2012).



AMR ratio $\equiv \Delta\rho/\rho$

$$= \gamma(\rho_{\downarrow s_{\downarrow} \rightarrow d_{\uparrow}} - \rho_{\uparrow s_{\downarrow} \rightarrow d_{\downarrow}}) / \rho_{\uparrow\downarrow} + \rho_{\downarrow\uparrow}$$

$$\propto \gamma(D_{\uparrow}^{(d)} \uparrow - D_{\downarrow}^{(d)} \downarrow) (1/\rho_{\downarrow})$$

with

$$\rho_{\downarrow\sigma} = \rho_{\downarrow s_{\downarrow} \rightarrow \sigma} + \rho_{\downarrow s_{\uparrow} \rightarrow \sigma} \rightarrow d_{\sigma}$$

$$\gamma = (3/4)(\lambda/H_{\text{ex}}) \uparrow^2$$

$\rho_{\downarrow\sigma}$: Resistivity of σ spin

$D_{\uparrow}^{(d)}$: Density of states of d -electron

λ : Spin-orbit coupling constant

H_{ex} : exchange field of the d -states

Half-metallic materials

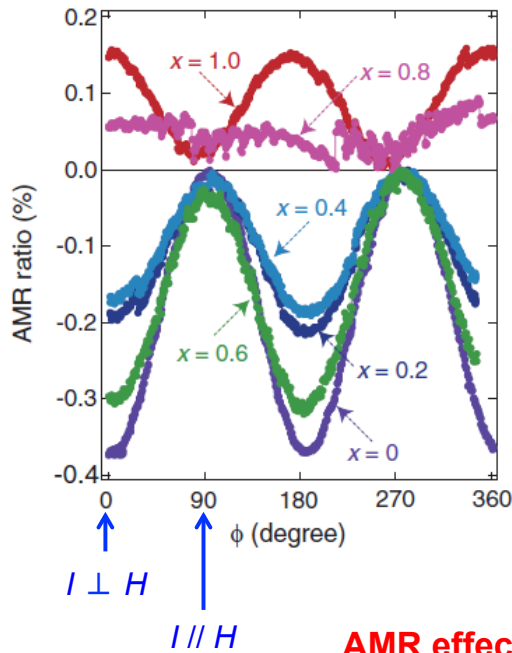


Negative sign of AMR ratio

10

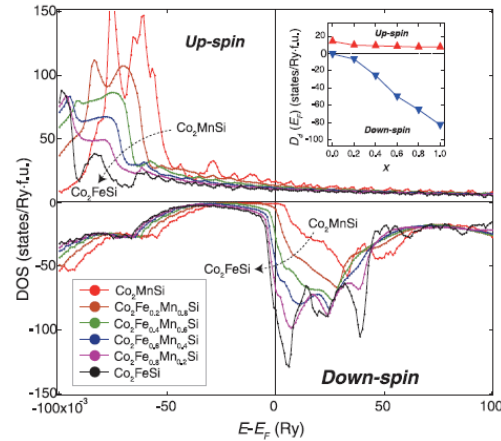
AMR effects of Heusler alloy films

AMR curves of $\text{Co}_2\text{Fe}_x\text{Mn}_{1-x}\text{Si}$ films



Yang, Sakuraba, KT, *et al.*, PRB **86**, 020409(R) (2012).

DOS of $\text{Co}_2\text{Fe}_x\text{Mn}_{1-x}\text{Si}$ alloys (calc.)

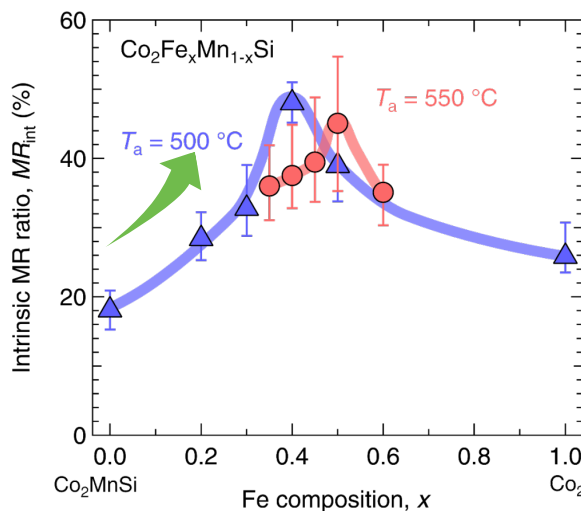


AMR effect is a fingerprint for half-metallicity.

11

CPP-GMR with $\text{Co}_2\text{Fe}_x\text{Mn}_{1-x}\text{Si}$ electrodes

Discussion - Fe:Mn composition ratio x dependence



Calculated exchange stiffness by first-principles calculations (Dr. Miura, Tohoku univ.)

Exchange stiffness of Co [meV]	$\text{Co}_2\text{MnSi}/\text{Ag}$	$\text{Co}_2\text{FeSi}/\text{Ag}$
Interface	137	340 (x 2.5)
Bulk	414	536

bulk spin-asymmetry interface spin-asymmetry

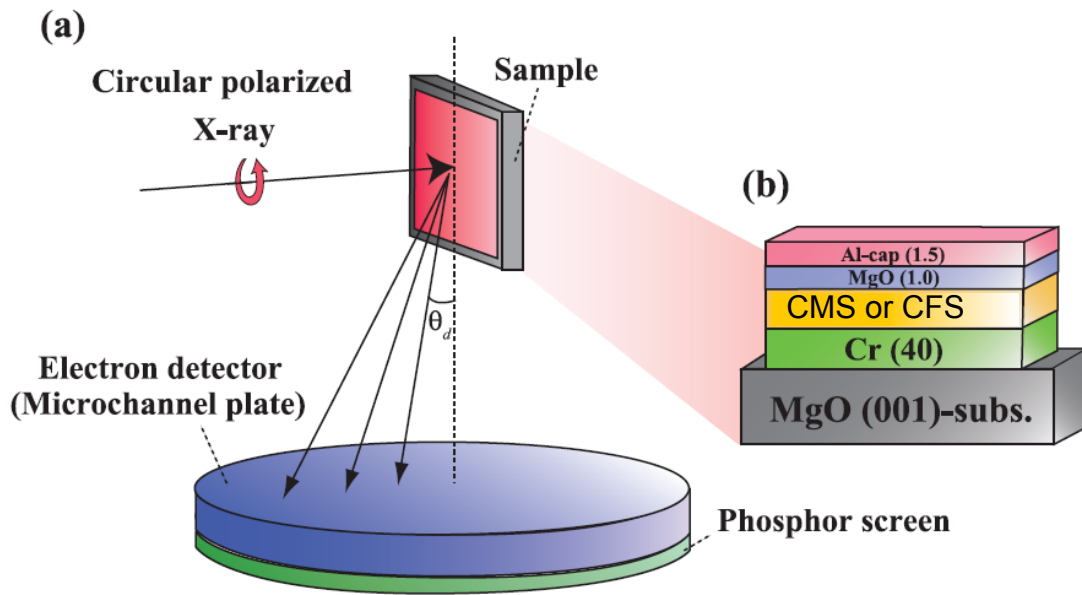
$$\Delta RA \propto \left(\underbrace{\beta \rho_{CFMS}^* t_{CFMS}}_{\text{bulk contribution}} + \underbrace{\gamma R_{CFMS/Ag}^* A}_{\text{Interface contribution}} \right)^2$$

Systematic analysis of γ is necessary to clarify the improvement of interfacial exchange stiffness.

12

Depth-resolved XMCD measurements

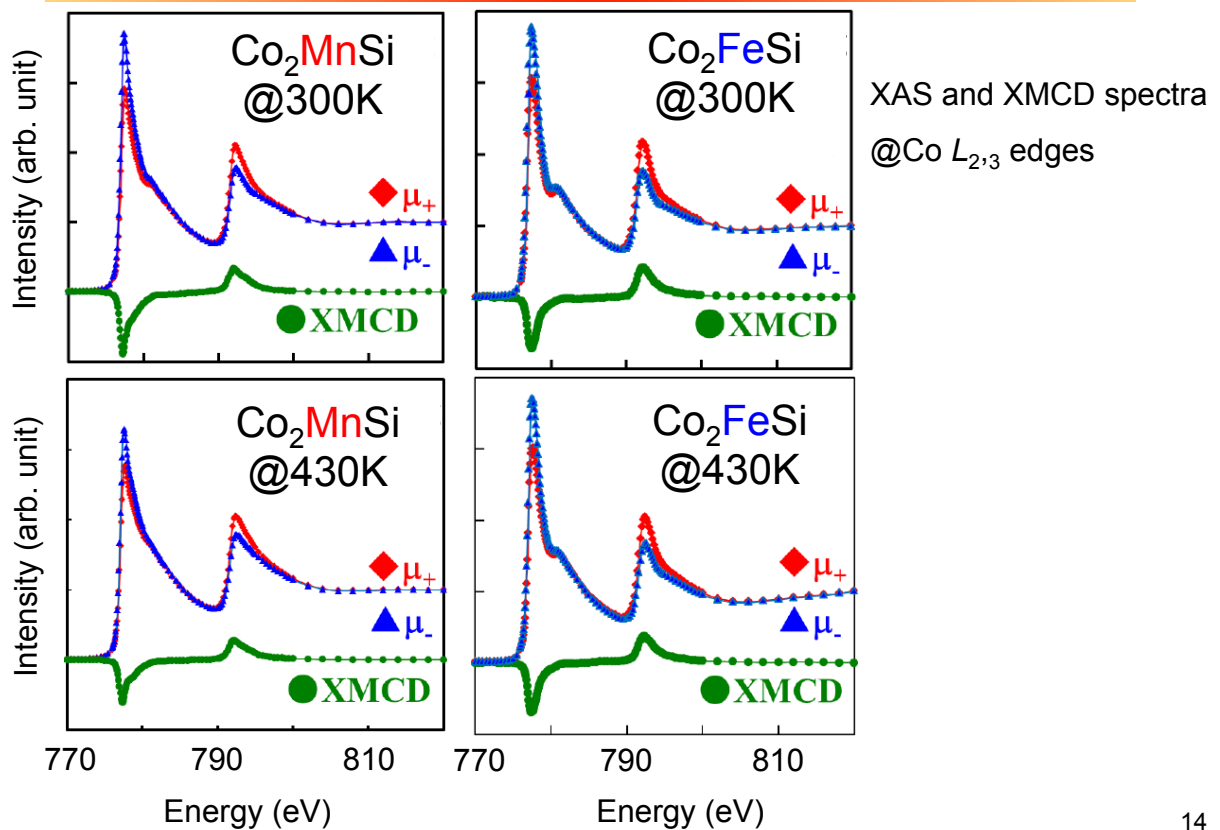
Measured@BL-16A, Photon Factory, KEK
 Collaboration with Prof. Amemiya, Dr. Sakamaki



Soft x-ray \rightarrow penetration depth (~ 5 nm or less)
 Depth-dependence of magnetic moments can be measured.

13

Exchange stiffness constants at interfaces



14

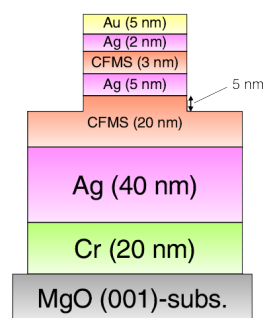
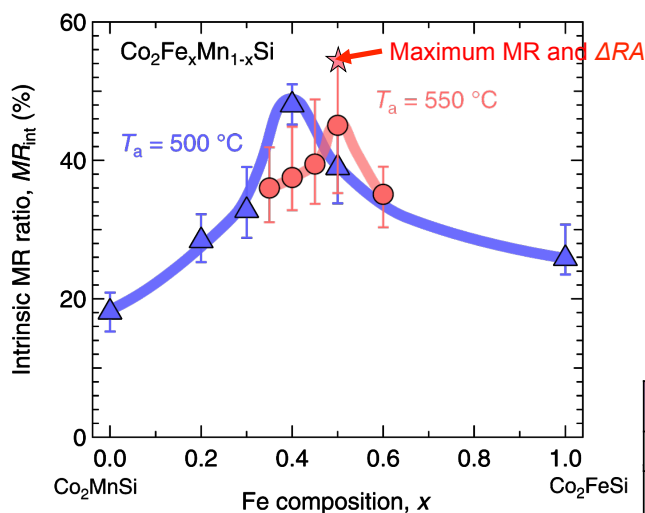
“Bulk” moment & “Interface” moment

Temperature dependence of Co-moment at the interface;
Larger for the $\text{Co}_2\text{MnSi}/\text{Ag}$ case than that for the $\text{Co}_2\text{FeSi}/\text{Ag}$ case

15

CPP-GMR with $\text{Co}_2\text{Fe}_x\text{Mn}_{1-x}\text{Si}$ electrodes

Fe:Mn composition ratio x dependence



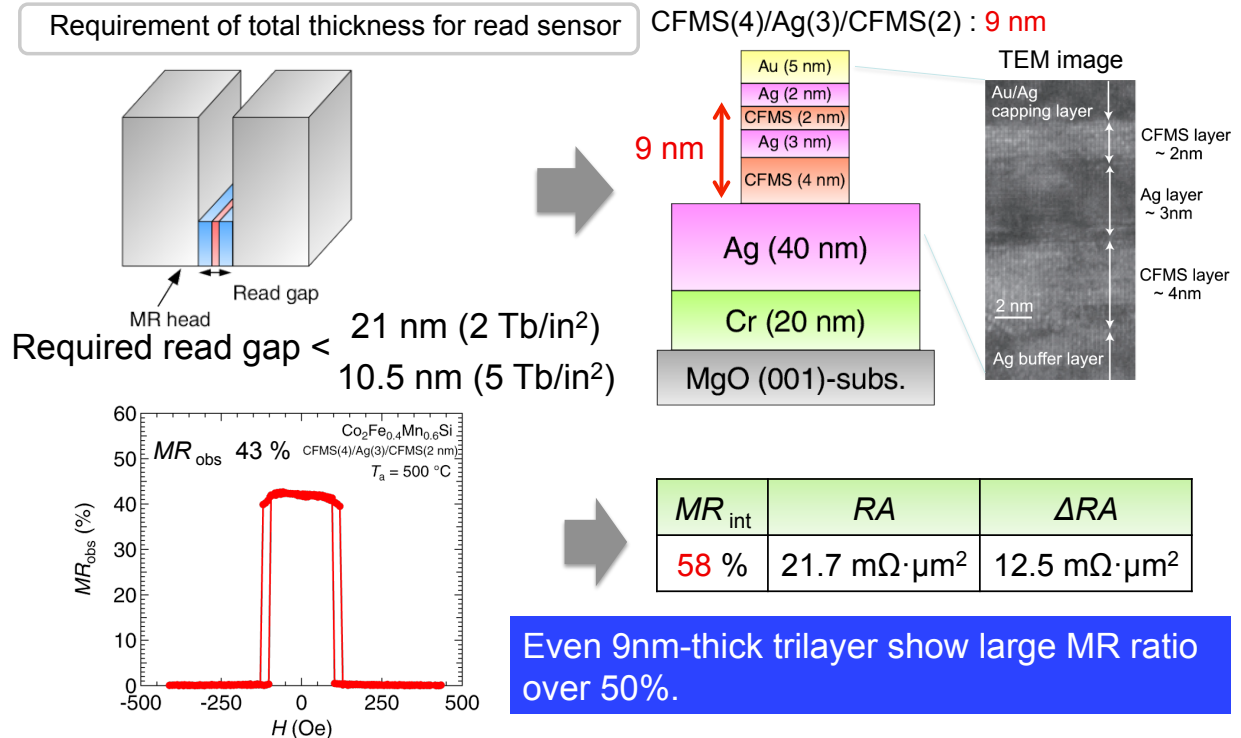
T_a	x_{best}	MR_{int}	RA	ΔRA
500	0.4	51 %	$25.1 \text{ m}\Omega \cdot \mu\text{m}^2$	$12.8 \text{ m}\Omega \cdot \mu\text{m}^2$
550	0.5	55 %	$31.4 \text{ m}\Omega \cdot \mu\text{m}^2$	$17.2 \text{ m}\Omega \cdot \mu\text{m}^2$

Y. Sakuraba, M. Ueda *et al.* Appl. Phys. Lett. **101**, 252408(2012).

$x = 0 \rightarrow 0.5$: Interface contribution increases \rightarrow MR increases.
 $x = 0.5 \rightarrow 1$: Half-metallicity disappears \rightarrow MR decreases.

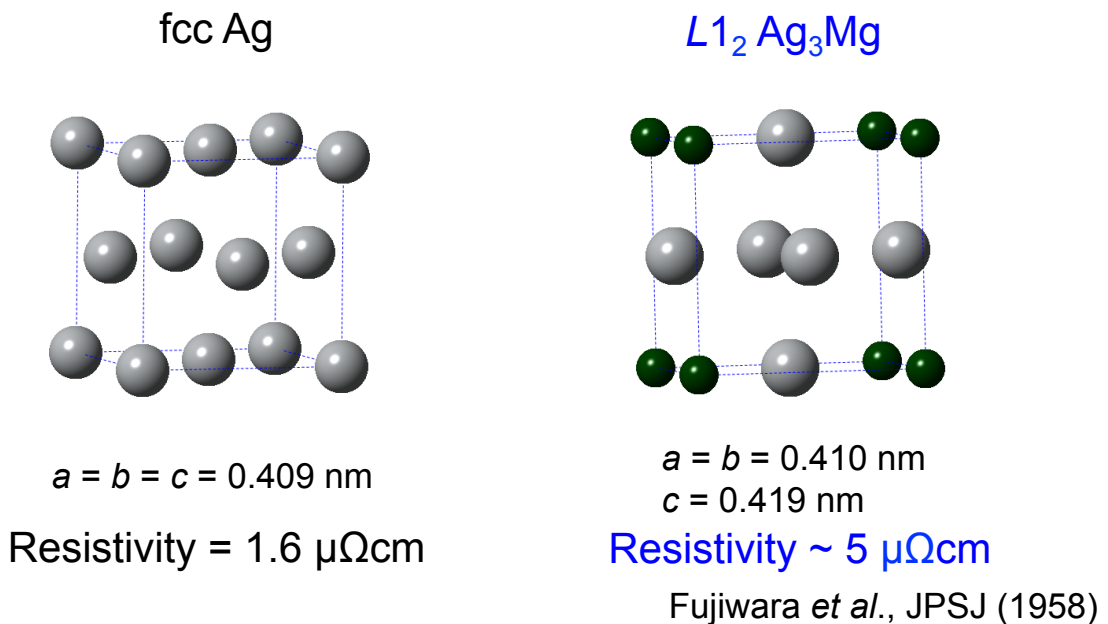
16

Challenge for a thinner layer thickness



17

Approach for higher output –new spacer material–

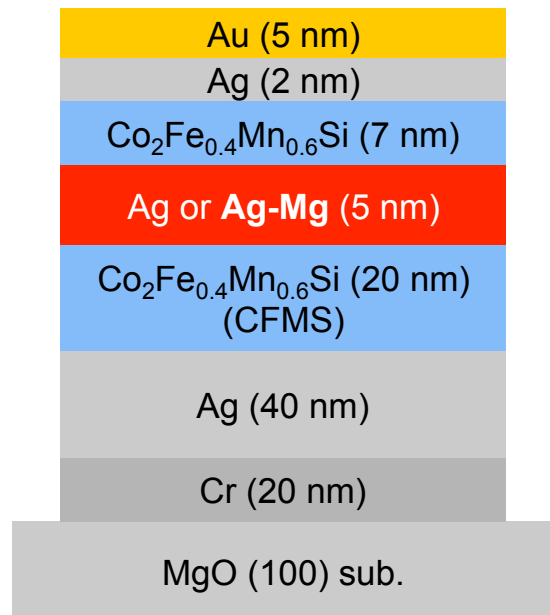


Lattice mismatch is similar (Ag ~ 2%, $L1_2 \text{Ag}_3\text{Mg}$ ~ 3%).

18

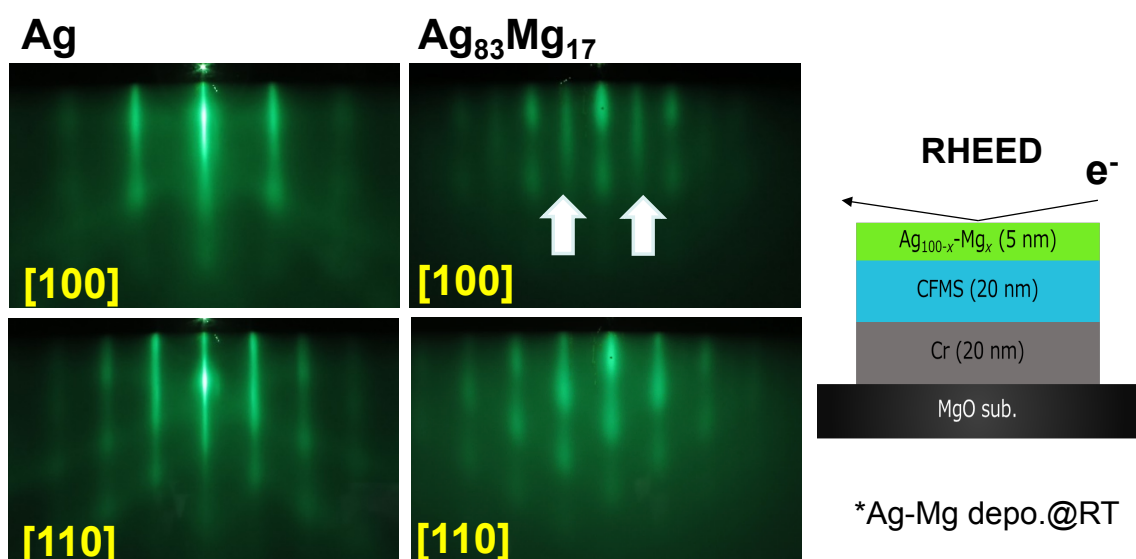
Experimental procedures

- Film deposition: Magnetron sputtering
- *In situ* annealing
 - @650°C after the Cr depo.
 - @500°C after the top CFMS depo.
- Ag-Mg layer
 - Deposited by co-sputtering
- Fabrication of CPP-pillar:
 - Electron-beam lithography & Ar ion dry etching
- Characterization:
 - XRD, RHEED,
 - Direct-current 4-probe measurement



19

RHEED patterns of a thin Ag-Mg film

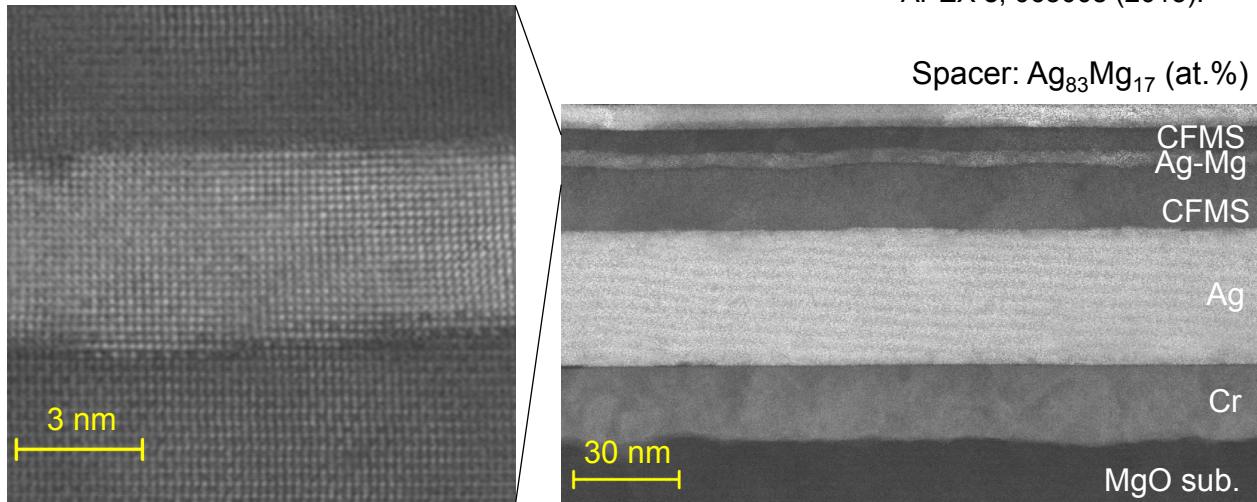


Superlattice diffraction was observed for the surface of Ag₈₃Mg₁₇ (~ Ag₅Mg) layer deposited at room temperature

20

Cross-sectional HAADF-STEM for Ag-Mg spacer

H. Narisawa, T. Kubota, KT, APEX 8, 063008 (2015).

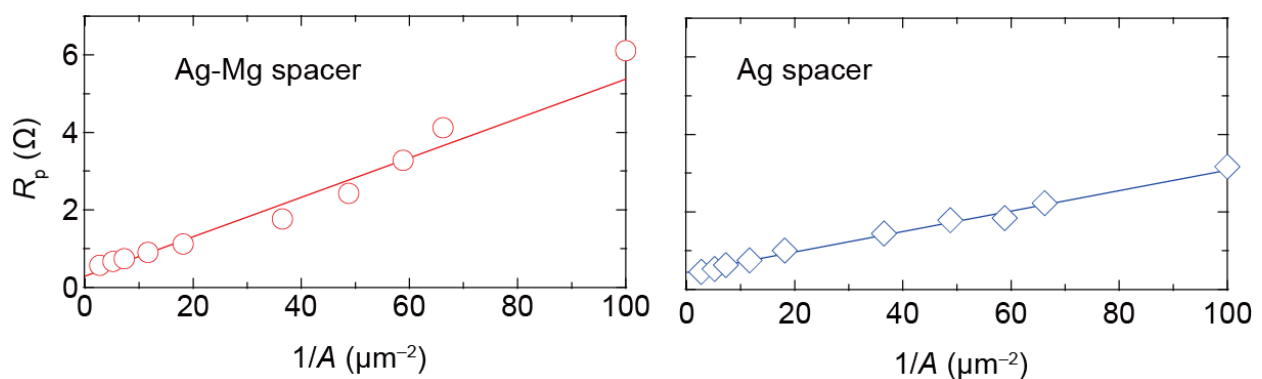


CFMS/Ag-Mg/CFMS → Flat and sharp interfaces

$\text{Ag}_{83}\text{Mg}_{17}$ spacer layer → Ordered locally at interfaces

21

RA in CFMS/Ag/CFMS



$$RA = 51 \pm 4 \text{ m}\Omega\mu\text{m}^2$$

$$R_{\text{para}} = 0.30 \pm 0.14 \Omega$$

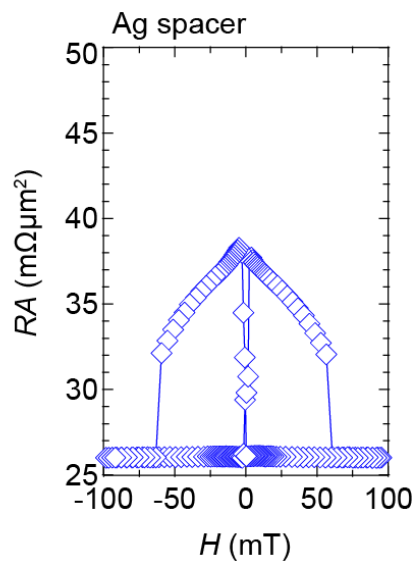
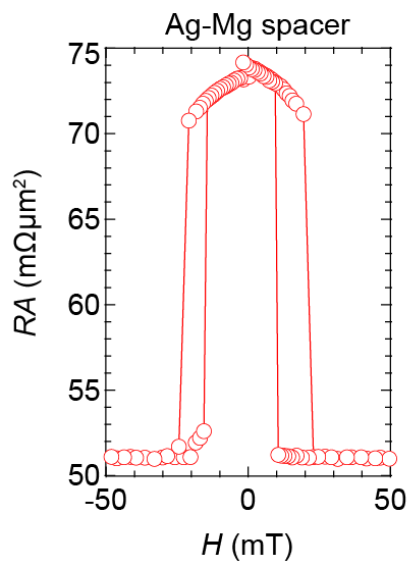
$$RA = 26 \pm 1 \text{ m}\Omega\mu\text{m}^2$$

$$R_{\text{para}} = 0.43 \pm 0.04 \Omega$$

RA for Ag-Mg spacer is twice larger than that for pure Ag spacer.

22

CPP-GMR in CFMS/Ag-Mg/CFMS



Large ΔRA for Ag-Mg compared to that for Ag

$$*MR_{\text{int}} = \Delta R / (R_p - R_{\text{para}})$$

Spacer	RA (mΩμm ²)	MR _{obs} (%)	MR _{int} (%)	ΔRA (mΩμm ²)
Ag	26	35 (38)	48 (54)	13 (15)
L1 ₂ Ag-Mg	51	36 (40)	44 (48)	23 (25)

23

Temperature dependence of CPP-GMR

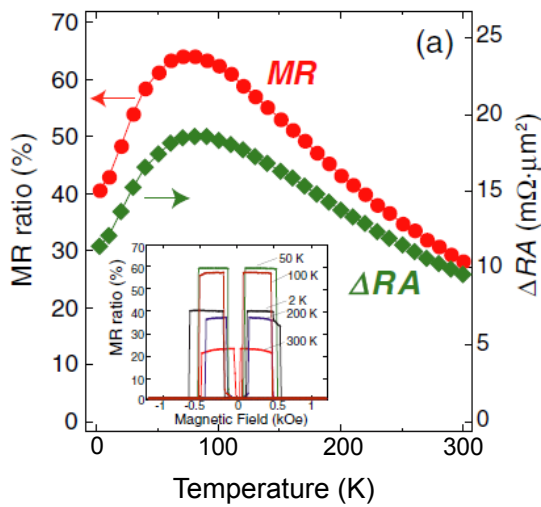
Ag spacer
→ Maximum ~80 K

Ag-Mg spacer
→ Maximum disappears.

24

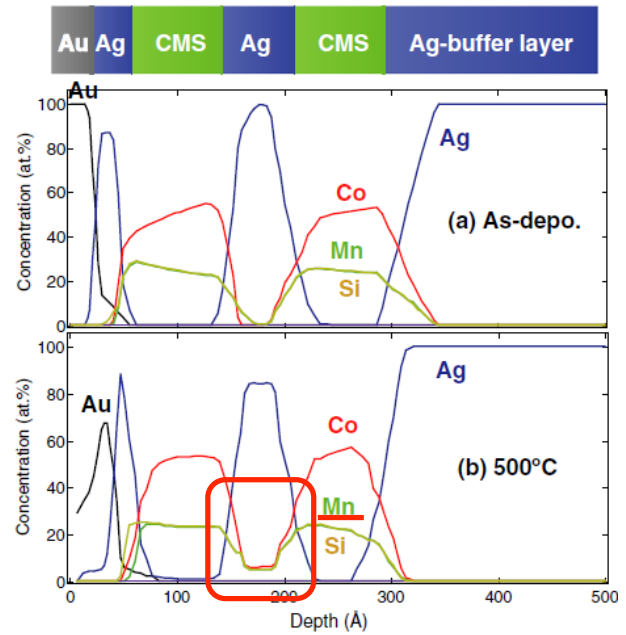
Temp. dependence; effect of Mn-diffusion

Previous work on
 $\text{Co}_2\text{MnSi}/\text{Ag}/\text{Co}_2\text{MnSi}$



Diffusion of Mn probably causes a maximum of the temp. dependence.

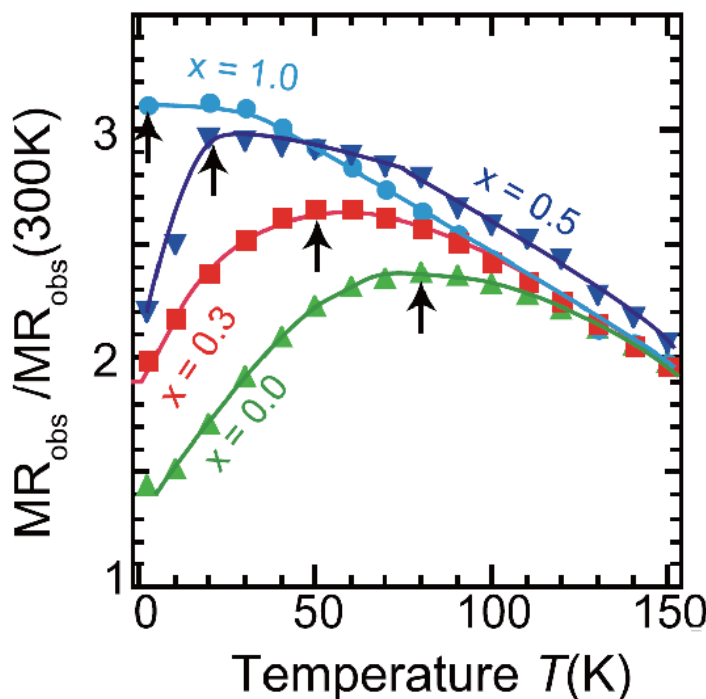
Depth profiles of the film composition (RBS)



Y. Sakuraba, *et al.*, J. Phys. D. (2011).

25

Temperature dependence of CPP-GMR



$\text{Co}_2\text{Fe}_x\text{Mn}_{1-x}\text{Si}$

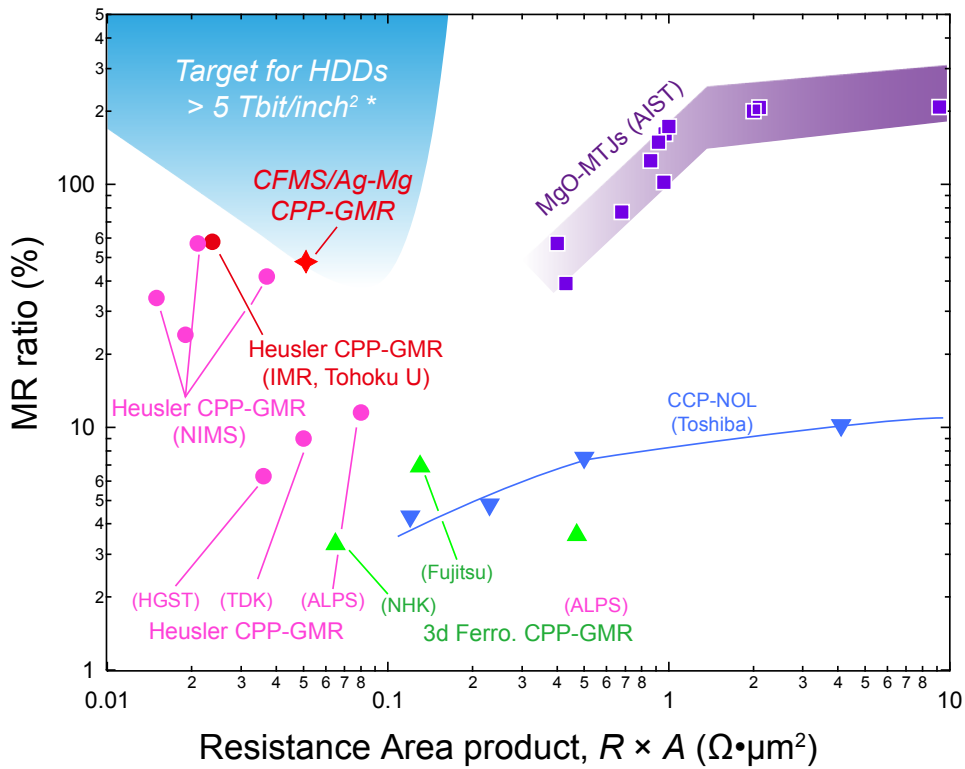
Y. Sakuaba, KT, *et al.*,
Appl. Phys. Lett. **101**, 252408 (2012).

Related to Kondo physics?

L. O'Brien *et al.*,
Nature Commun., 5:3927 (2014).

26

High MR ratio with low resistance

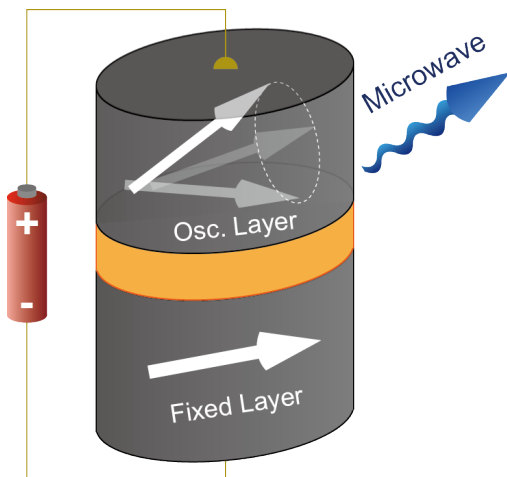


28

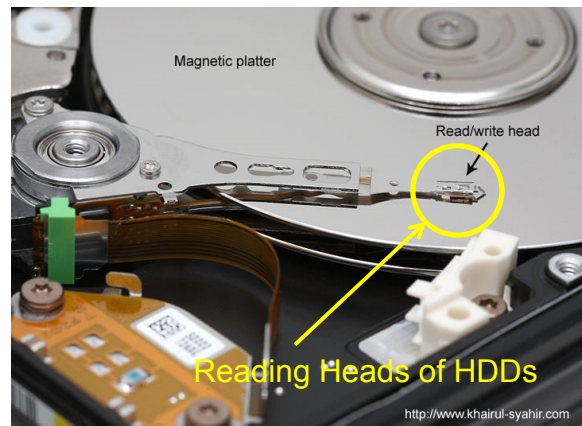
Device applications using CPP-GMR devices

Heusler-alloy-based CPP-GMR devices

Spin torque oscillators



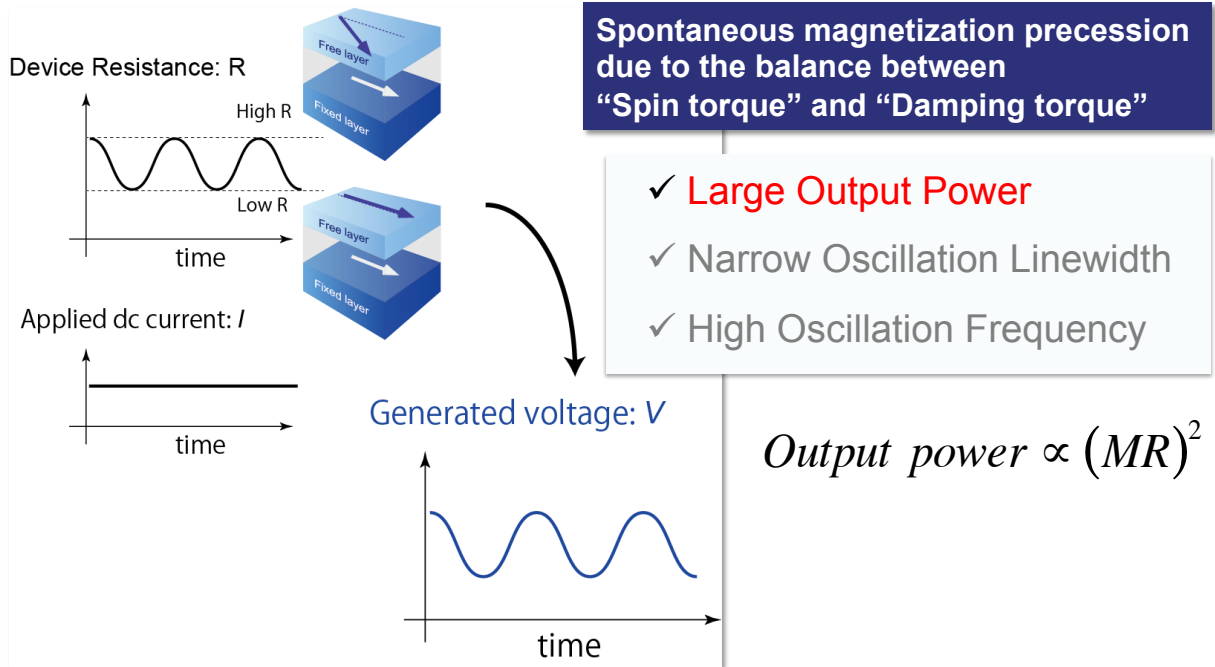
Read Heads in HDDs



29

Spin torque oscillator (STO)

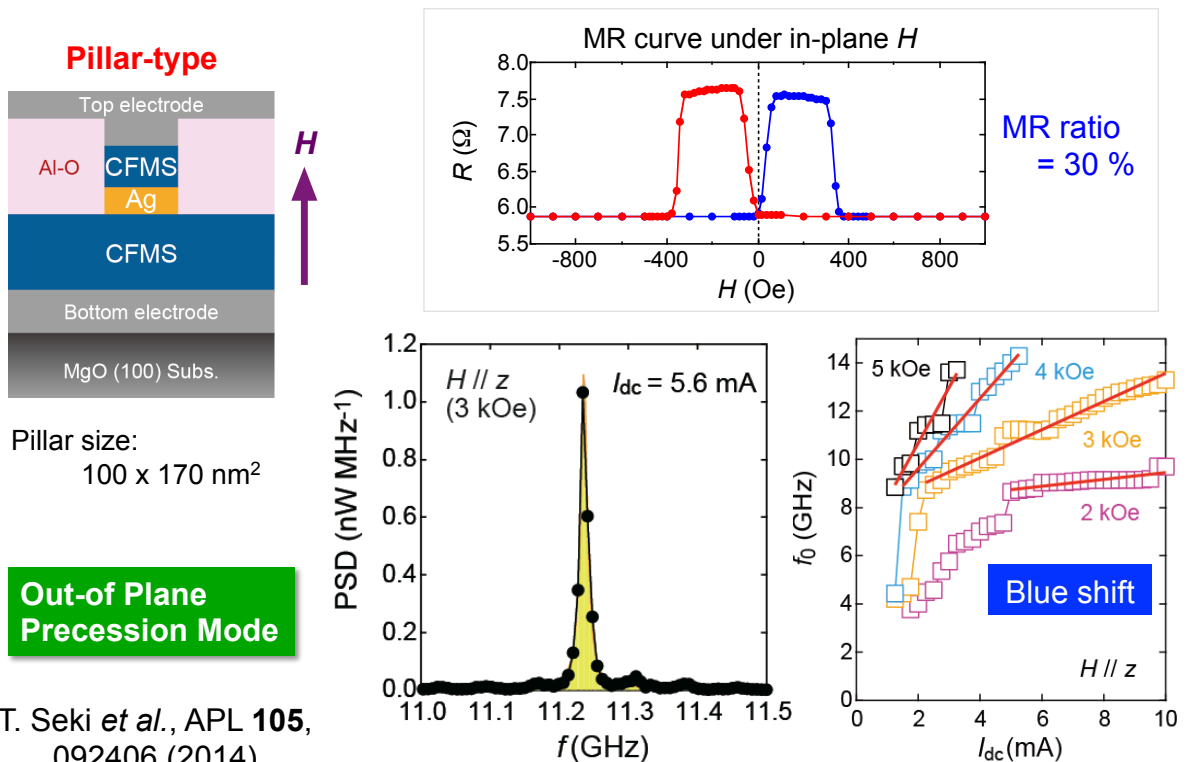
What is Spin Torque Oscillation?



Half-metallic Heusler alloy showing large MR

30

Heusler CPP-GMR STO (Pillar)



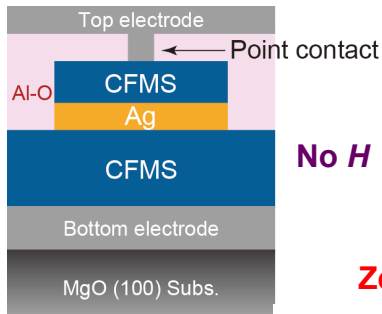
T. Seki *et al.*, APL **105**, 092406 (2014)

$P_{out} = 23.7 \text{ nW}, Q = 1124$

31

Heusler CPP-GMR STO (Point Contact)

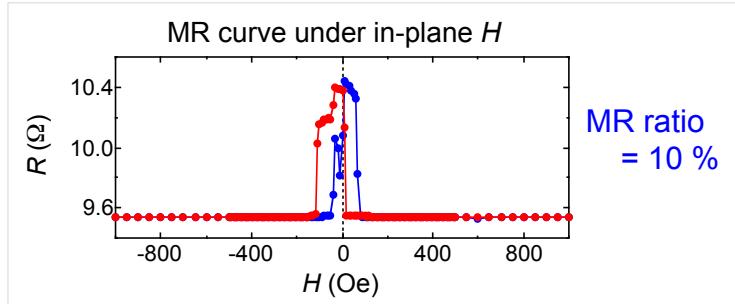
Point Contact-type



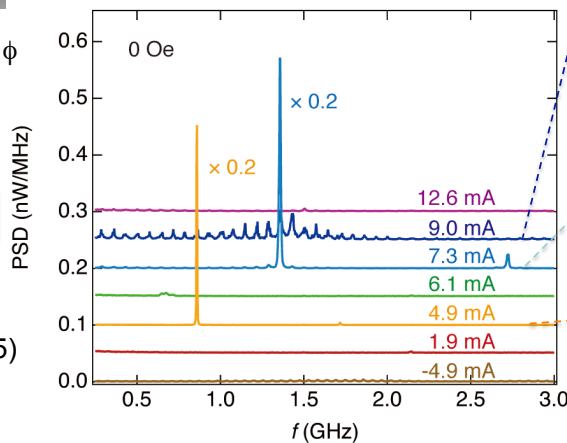
Contact size: 140 nm ϕ

Vortex-like Mode

T. Yamamoto *et al.*,
APL **106**, 092406 (2015)



Zero-field spin torque oscillation



Region III: Incoherent
Multiple peak structure
Chaotic dynamics?

Region II: Coherent
 $f_0 = 1.36$ GHz
 $\Delta f = 9$ MHz

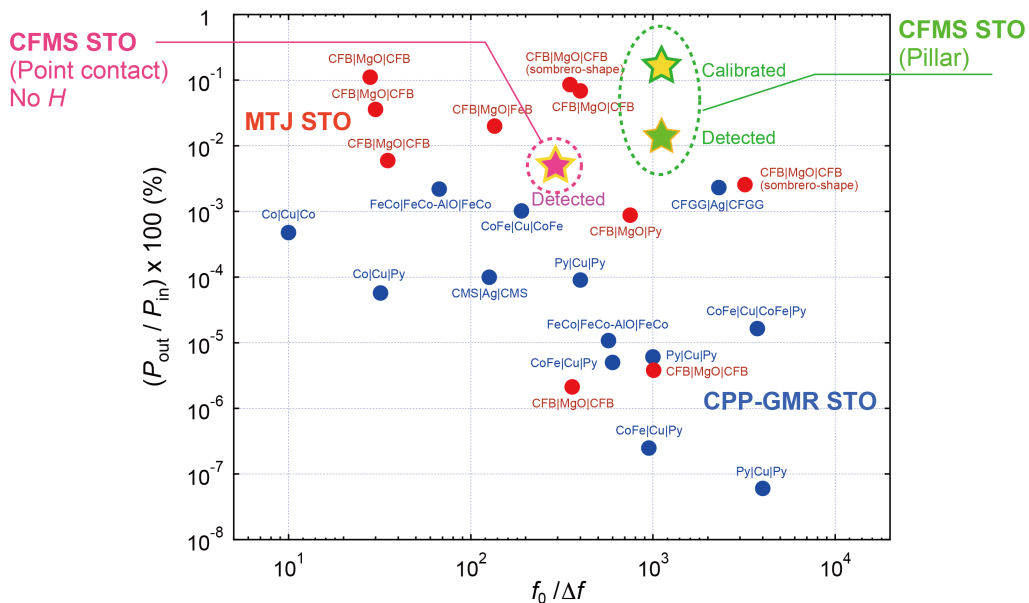
Region I: Coherent
 $f_0 = 0.86$ GHz
 $\Delta f = 3$ MHz

32

Heusler CPP-GMR STO

Nanopillar	$P_{out} = 23.7$ nW	$\Delta f = 10$ MHz	$H = 3$ kOe ($//z$)
T. Seki <i>et al.</i> , APL 105 , 092406 (2014)			
Point Contact	$P_{out} = 11.6$ nW	$\Delta f = 3$ MHz	$H = 0$ Oe

T. Yamamoto *et al.*, APL **106**, 092406 (2015)



33

Summary

Half-metallic Heusler alloys for spintronics

- **CPP-GMR in $\text{Co}_2\text{Fe}_x\text{Mn}_{1-x}\text{Si}/\text{Ag}/\text{Co}_2\text{Fe}_x\text{Mn}_{1-x}\text{Si}$**
 - **Composition dependence:**
Max. of CPP-GMR @ $x=0.4\sim 0.5$
 - **Spacer: Ag \rightarrow Ag-Mg**
Enhancement of ΔRA
 - **Temperature dependence of CPP-GMR**
Maximum for CMS/Ag/CMS, CFMS/Ag/CFMS
No Maximum for CFS/Ag/CFS, CFMS/Ag-Mg/CFMS
- **STO with CPP-GMR devices with CFMS/Ag/CFMS**
 - **nanopillar-type; high output power and high Q**
 - **point contact-type; high output power and high Q with no applied field**

33

Magnetic Materials Laboratory

Lab members

Professor Koki Takanashi

Assoc. Prof. Masaki Mizuguchi

Assist. Prof. Takeshi Seki

Takahide Kubota

Post-doc. Zenchao Wen

Hitomi Yako

DC students Wei-Nan Zhou (China)

Jinhyeok Kim (Korea)

Takayuki Tashiro, Tatsuya Yamamoto, Tomoki Tsuchiya

MC students Junpei Shimada, Mingling Sun (China)

Yusuke Ina, Satoru Kikushima, Hidenobu Suzuki,



Collaborators on Heusler work

Tomoko Sugiyama (IMR, Tohoku Univ.)

Yuya Sakuraba, Subrojati Bosu (NIMS, Tsukuba)

Masafumi Shirai (RIEC, Tohoku Univ.), Yoshio Miura (Kyoto Institute of Technology)

34